Plasma Physics and Controlled Fusion

Excited-state potentials for modelling dense plasmas from first principles

To cite this article before publication: Patrick James Hollebon *et al* 2021 *Plasma Phys. Control. Fusion* in press https://doi.org/10.1088/1361-6587/ac2615

Excited-state potentials for modelling dense plasmas from first principles

P. Hollebon[1], J. S. Wark[1], S. M. Vinko[1,2]

[1] Department of Physics, Clarendon Laboratory, University of Oxford, Parks Road, Oxford OX1 3PU, UK

[2] Central Laser Facility, STFC Rutherford Appleton Laboratory, Didcot OX11 0QX, UK

E-mail: phollebon@lanl.gov

April 2021

Abstract. The modelling of dense plasmas using finite-temperature density functional theory has proven very successful in determining transport properties and the equation of state of systems where quantum many-body effects and correlations play a key role in their structure. Here we show how excited-state projector augmented-wave potentials can be used to extend these calculations to explicitly model core-hole states, allowing for the calculation of the electronic structure of a range of integer charge configurations embedded in a dense plasma environment. Our excited-state potentials show good agreement with all-electron calculations at finite-temperatures, motivating their use as an efficient approach in modelling from first principles both the structure of strongly-coupled non-equilibrium plasmas and their interaction with intense X-rays.

1. Introduction

The computational study of dense, strongly-coupled plasmas has benefited immensely from the application of density functional theory (DFT) [1], within both single-centre average atom approximations [2–4] and in combination with molecular dynamics to form true multi-centred models [5]. Plasma investigations based on DFT are ideal in these conditions as they offer a fully quantum-mechanical, in principle exact, approach to the many-body problem whilst requiring a minimal set of approximations. Crucially, they yield results consistent with experiment.

Optimising the efficiency of these simulations is of great practical importance. In principle, DFT is capable of providing the structure for all the electrons present in the system under study. In practice, however, it is often convenient to separate the electrons into two groups: core and valence. The core electrons of an ion are those which do not interact with the electrons of other ions, and therefore do not play a role in the chemistry of the system. The valence electrons are, in turn, those which do interact with other electrons, and give rise to bonding, structure, electrical conductivity,

and a range of other properties. In the condensed matter ground state relatively few electrons participate in the chemistry, and the large number of core electrons can be conveniently excluded from the explicit DFT calculation, and modelled via an effective pseudopotential. When possible, the use of pseudopotentials can significantly increase the efficiency of calculations [6].

An important aspect of a plasma is that it is composed of a distribution of ion charge states, which, in equilibrium, is determined uniquely by the temperature and density of the system. Such an equilibrium plasma can be modelled with finite-temperature DFT [7], albeit at considerable computational expense, and often still only up to moderate temperatures on the order of the Fermi energy of the system, generally around 10 eV, before additional approximations must be made [8]. Advances in computational capabilities now allow for efficient DFT simulations of systems containing over 10,000 atoms [9]. Whilst this does not yet approach the size of a plasma generated experimentally (e.g., a cubic micron of solid-density Al contains about 6×10^{10} atoms), when coupled with molecular dynamics (MD) such calculations are becoming large enough to encompass a true ensemble of ions necessary for a proper thermodynamic treatment of dense plasma properties [10]. Finite temperature DFT-MD combined with linear response theory has been successfully applied to study a range of plasma properties such as the equation of state [11–20], structure factors [21, 22], phases and phase transitions [23], electrical conductivities [24–26], opacities [27, 28], optical properties [29, 30], and entropies [31], and are important tools for a wide range of investigations in planetary physics [13, 32] and inertial confinement fusion [24].

Thus far calculations remain limited in that whilst one can explicitly model an ensemble of ion positions, for example corresponding to individual time steps of an MD simulation, the resulting system remains a thermal average calculation with the computed electron density $\rho(\mathbf{r})$ corresponding to the ensemble average over electronic microstates for each ion arrangement. Within finite temperature Kohn-Sham (K-S) DFT [33] this is expressed in terms of the non-interacting K-S orbitals $\Psi(\mathbf{r})$, populated by the Fermi-Dirac distribution $f_i(\epsilon_i - \mu)$:

$$\rho(\mathbf{r}) = \sum_i f_i(\epsilon_i - \mu)|\Psi_i(\mathbf{r})|^2. \quad (1)$$

Equation 1 lacks a description of thermal fluctuations in the electron density, the resulting charge state variations from ion to ion, and the role of a locally varying microfield [34, 35] on plasma properties. Such inhomogeneities can have profound impacts on electronic transport properties [36–38]. By design, the Kohn-Sham system also hides the complicated electronic correlations needed to describe interaction driven localisation and the transition between bound and free states [39–41]. Excited-state, frozen-core pseudopotentials offer a computationally cheap means to avoid these limitations by modelling the interaction of specific ion charge states with the surrounding plasma. Such an approach enables one to explicitly account for the distribution of ion

charge states with a plasma by populating a supercell with a variety of excited state potentials, each corresponding to different ion charge states present within the plasma. Importantly, while the pseudopotentials are designed to represent an excited state, the DFT calculation remains a ground state or finite temperature calculation, constrained to provide the minimum energy solution for the electron density distribution under the boundary conditions of the excited-core pseudopotential.

The use of excited-state pseudopotentials to model various ion configurations has allowed researchers to interpret results from photoemission spectroscopy [42–44], XANES [45–47], and X-ray emission spectroscopy [48, 49]. Generally speaking, this capability is important for all applications where the specific charge state of the individual ion within the plasmas matters. A prime example of this is recent research on the physics of ionization potential depression [50–52], and studies investigating the electronic structure of dense plasmas using x-ray scattering [53–55]. However there remains no simple and rigourous scheme for modelling the interaction of an excited ion with a surrounding plasma in DFT, nor is there any guarantee that a DFT supercell calculation containing a variety of such potentials should result in anything physically meaningful. Ground state pseudopotentials on the other hand are generally tested by comparing the produced band structures and densities of states (DOS) with the respective all-electron calculations.

Here we present a verification procedure that extends this test to excited-state Na pseudopotentials, by performing a consistency test with finite-temperature all-electron calculations. Excited-state pseudopotentials would be appealing across the periodic table, however Na in particular serves as an excellent test case by having both sufficiently electrons that a finite temperature, all-electron calculation is feasible whilst also possessing sufficiently inactive K and L shells that they may be frozen in the core. Using the finite-temperature plane-wave DFT code Abinit [56], we have calculated the DOS for a range of Na ion charge states using Projector Augmented Wave (PAW) potentials [57] for a crystalline unit cell of solid-density Na. We compare the calculation performed using frozen-core potentials of excited states containing core holes with all-electron calculations at temperatures sufficient to vacate core states thermally, as described by the Fermi-Dirac distribution. The temperatures and the excited state configurations are specifically chosen to create systems with consistent shell populations that can be compared directly. We observe excellent agreement in the calculated electronic structure using the two types of pseudopotentials. While this does not necessarily guarantee the excited state pseudopotentials produce physically correct results, it does ensure that the introduction of the pseudopotential in the DFT calculation, and the freezing of excited core states, has a negligible impact on the results obtained.

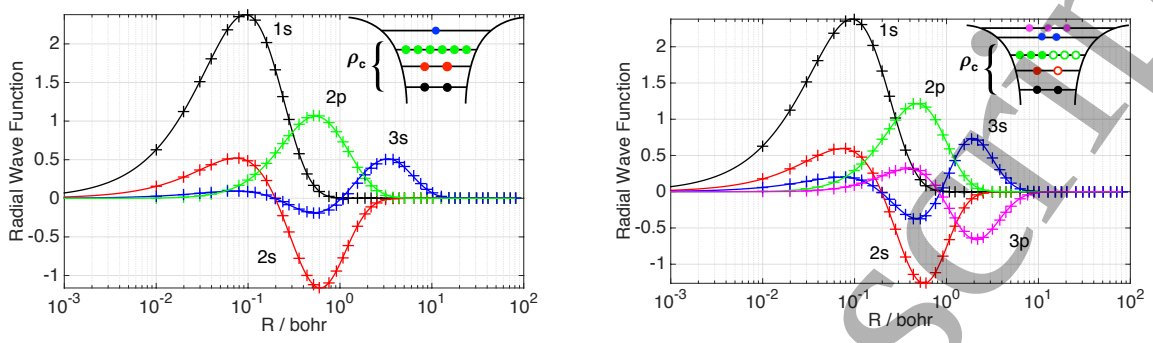

(a) Ground State (b) 4 electrons ionised out of core K L shells

Figure 1: (Colour online) Hartree-Fock (+) vs Kohn-Sham (solid lines) orbitals for isolated Na atoms

2. Excited State PAW potentials

Mindful as we are of the importance a proper treatment of the ion charge state distribution may have for transport coefficients, and of the distinction between bound and free states, we have chosen to construct our excited state potentials using the PAW formalism. Within this formalism the computationally difficult, highly oscillatory valence wavefunction behaviour close to the ion is smoothed with a transformation analogous to a change of basis. Unlike other pseudopotential methods this, in principle, does not lead to any approximation of the valence state behaviour beyond those afforded by the frozen core approximation. No presumptions are made concerning whether the valence states are bound or free, and close to the ion the K-S wavefunctions can be reconstructed, complete with rapid oscillations, by inverting the transformation.

Our frozen core pseudopotentials are constructed using the Atompaw [58] code by first performing an all-electron DFT calculation for the isolated Na atom. We take the three lowest lying K-S states (i.e. those resembling 1s, 2s and 2p atomic orbitals) as the core to be frozen. Excited core potentials are generated by artificially enforcing non ground state occupation numbers on the three lowest lying K-S states with charge neutrality maintained by placing an appropriate number of electrons into valence states, in the 3s and 3p orbitals. The system is then allowed to relax to minimise its total energy subject to the constraint of the excited frozen core configuration.

Which excited configurations we can test is somewhat limited by the need to have a sensible reference result. Fortunately, whilst an explicit calculation of a generic excited state within DFT is difficult, a finite temperature result can be obtained by minimising the Mermin free energy functional. A finite temperature DFT calculation using all-electron PAW yields, in principle, an exact solution for thermal ensemble average quantities derivable from the electron density to within the accuracy of the exchange-

correlation functional used. For the specific case of a solid-density lattice of Na ions one expects thermal ionisation of the core 1s, 2s and 2p states as the electron temperature of the system is increased. An all-electron calculation at these temperatures thus provides a suitable reference with which to compare excited state pseudopotentials intended to represent ions with one or more vacant states in the core.

The key requirements for a good pseudopotential are computational gain and transferability. By design the pseudopotentials reproduce the all valence electron K-S eigenvalues for the isolated atom. PAW potential construction was subject to the commonly used tests of matching logarithmic derivatives, atomic excitation energies and optimisation of projector functions [58], though the latter remained high when constructing all-electron potentials. Nonetheless, given the lack of a rigorous physical interpretation of the resulting K-S wave-functions we consider it instructive to compare them with single particle wave-functions as calculated within the Hartree-Fock, single Slater determinant approximation using the Missing [59] interface to Cowan's code [60]. The two methods produce nearly identical single particle wave functions for all excited state pseudopotentials constructed, supporting the creation of a given ion electronic configuration by directly imposing the same occupation numbers on the K-S orbitals. Little visible change occurs in the atomic wave functions as electrons are taken out of the core L shell and placed into M shell valence states (Figures 1a and 1b). The small change that is noticeable (primarily in the 2p and 3s wave functions) involves a contraction of the wave functions radially for both K-S and Hartree-Fock orbitals.

3. DFT calculations for warm dense Na

DFT calculations in the bulk, body-centred cubic (bcc) Na lattice were performed using the Abinit code [56], with the PBE generalised gradient expansion for the exchange-correlation energy [61]. Accurate sampling of the Brillouin zone is achieved using shifted 32×32×32 Monkhorst pack grids [62] for charge states up to 2 electrons ionised out of the core K and L shells. 16×16×16 grids were used for 3 and 4 L shell electron hole potentials due to the otherwise impractical amount of memory needed to represent the increasing number of occupied bands.

DFT calculations of the Na bcc ground state using the all-electron potential PAW and with fully occupied frozen cores yield lattice constants of 4.21 Å and 4.22 Å respectively, in close agreement to the experimental value of 4.23 Å [63]. In addition, both produce consistent valence electron DOS as seen in Figure 2. Testing of excited state potentials begins by first performing finite temperature calculations of a fixed solid density bcc Na lattice using all-electron PAW potentials. The electron temperature is varied to thermally ionise integer numbers of electrons out of the three lowest lying K-S states of this bulk system. These all-electron results then serve as a reference with which to compare excited state potentials constructed to model ions of equivalent charge state. The latter have been constructed such that the enforced occupation numbers of the 1s, 2s and 2p core states replicate the thermal occupation of the three lowest lying K-S

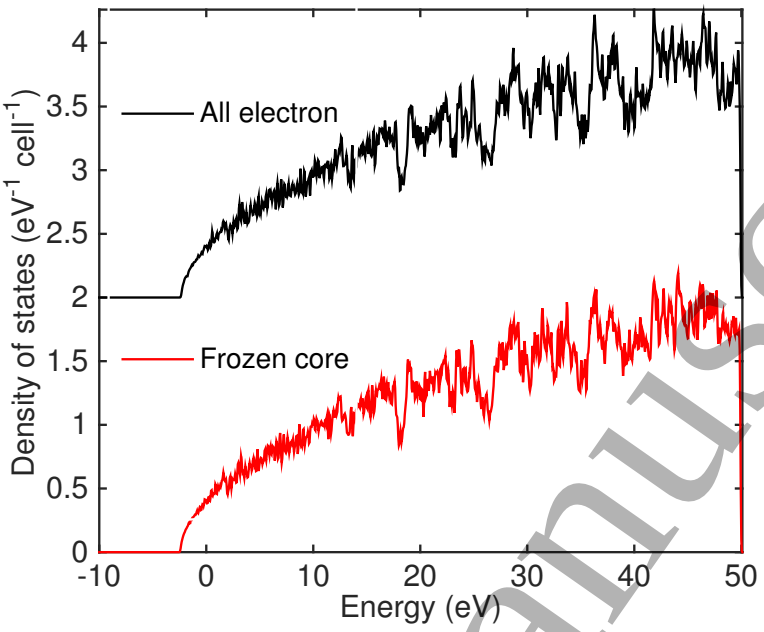

Figure 2: (Colour online) Valence DOS for ground state bulk bcc sodium. The $\sqrt{E}$ dependance characteristic of an ideal metal is clear.

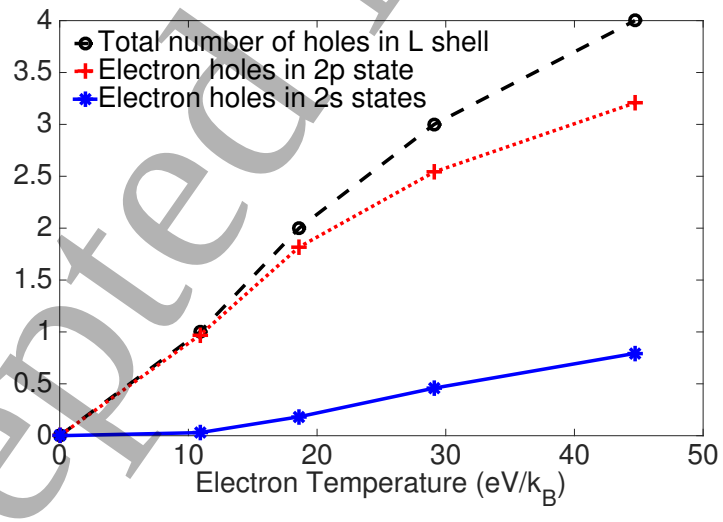

Figure 3: (Colour online) Electron temperatures thermally ionising integer numbers of electrons out of the L shell like Kohn-Sham orbitals, as calculated for a fixed bcc lattice of all-electron PAW potentials.

orbitals of the bulk all-electron calculation (see Figure 3).

A comparison of the resulting DOS for excited core and all-electron PAW potentials

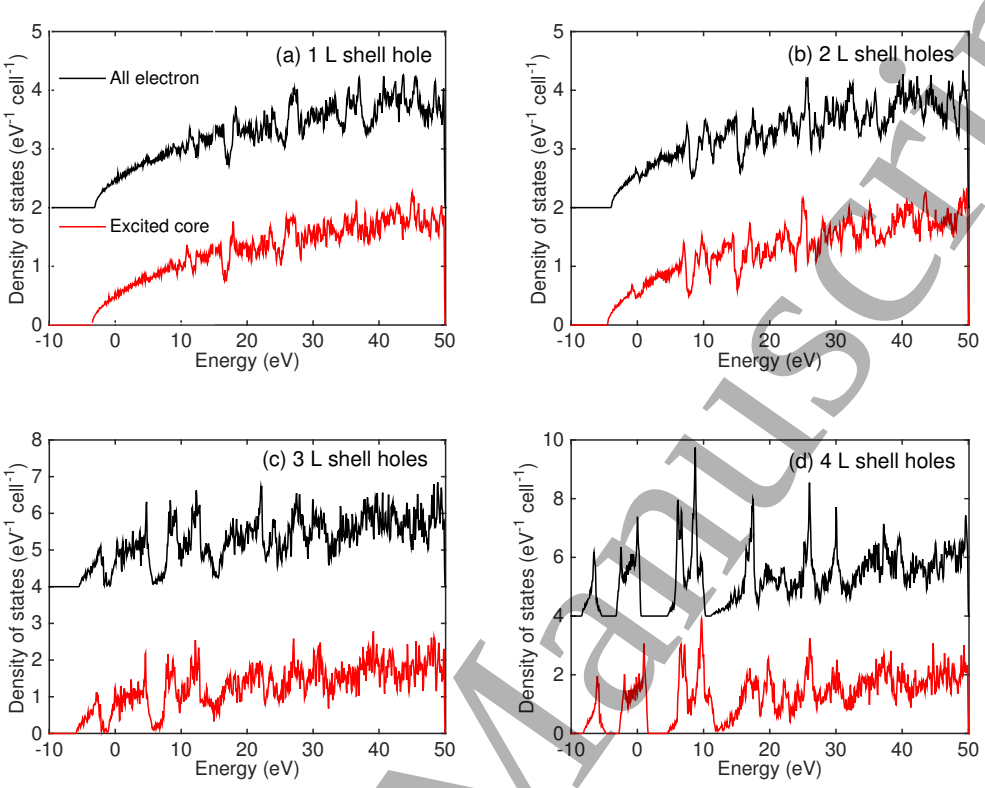

Figure 4: (Colour online) Electron temperatures thermally ionising integer numbers of electrons out of the L shell like Kohn-Sham orbitals, as calculated for a fixed bcc lattice of all-electron PAW potentials.

is shown in Figure 4. The angular momentum decomposition for 3 and 4 L shell holes is provided in Figures 5a and 5b, respectively. All DOS results have been converged with respect to the number of electron bands and auxiliary state plane wave basis set. Simulations for the 16 atom supercell of frozen core potentials produced DOS consistent with both all-electron and frozen core potentials in the primitive unit cell containing one atom. A continuous DOS is generated by using a Gaussian smearing function of full width half maximum 0.1 eV for each k point, except for the angular momentum projected DOS, for which the tetrahedron method is used. Note that in order to achieve a convergence in total energy of 0.5 eV the all-electron potentials required a plane wave basis cut off energy over six times higher than that for frozen core potentials ($\sim$ 410 eV compared with $\sim$ 2700 eV).

4. Discussion of results

From the DOS plots in Figure 4 it is apparent that the excited core PAW potentials do a good job of reproducing valence electron behaviour consistent with thermal average treatments based on finite temperature, all-electron PAW potentials. The implications

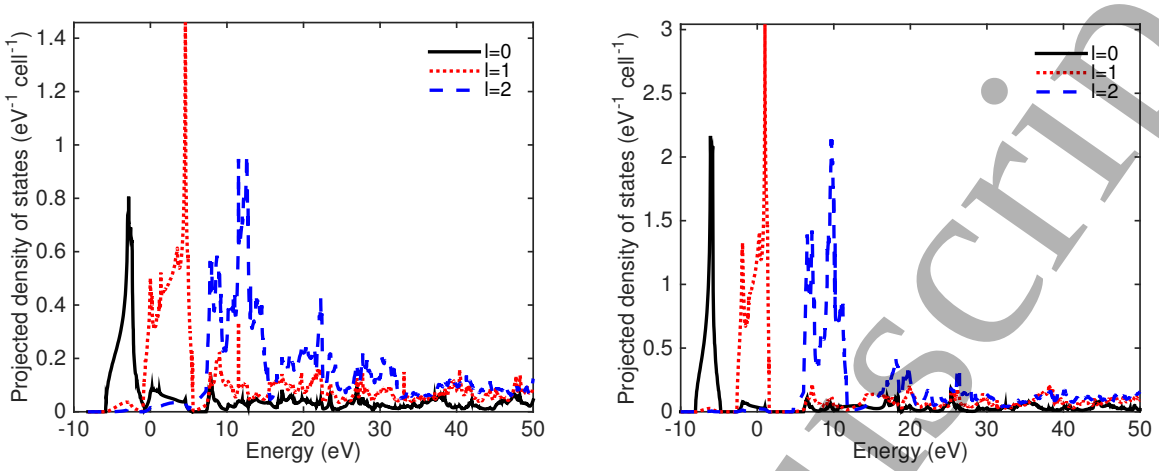

Figure 5: Angular momentum projected density of states within the PAW sphere for (a) 3, and (b), 4 electrons thermally ionised from the L shell respectively.

for this consistency are made clear when one considers the reasons why all-electron and the equivalent excited core calculations might, in general, be expected to disagree. For one, the core atomic K-S orbitals imported from the isolated atom calculation will necessarily differ from the low lying 1s, 2s and 2p states arising in the all-electron calculation in the bulk plasma, leading to a different ion potential experienced by the valence electrons. Second, even if the low lying all-electron K-S states are taken to constitute the frozen core the very act of freezing these states requires allowing the valence states to minimise the Mermin free energy functional Ω without accounting for the influence on core states. Expressing Ω in terms of it's components one has:

$$\Omega[\rho(\mathbf{r})] = T_s[\rho] + V_H[\rho] + V_{ext}[\rho] + E_{xc}[\rho] - TS[\rho].$$

Substituting $\rho = \rho_{core} + \rho_{valence}$ and minimising Ω with respect to variations in $\rho_{valence}$ would be the strictly rigorous approach. Due to the linear nature of the Coulomb interaction the sum of the Hartree term, $V_H[\rho]$, and external potential, $V_{ext}[\rho]$, is unchanged by the substitution, whilst the exchange correlation functional, $E_{xc}[\rho]$, is typically approximated as an explicit functional of ρ and so can be modified accordingly. A slightly more involved treatment of the non-interacting kinetic energy term $T_s[\rho_{core} + \rho_{valence}]$ based on perturbation theory has been used to estimate errors in ground state DFT calculations [64], however this involves relaxing the enforcement of orthogonality between core and valence states that is intrinsic to the PAW potential method. The results presented here extend this by explicitly demonstrating the freezing of the core to have only a small effect on the valence electron DOS for each excited state PAW potential under consideration, within a hot and dense plasma environment.

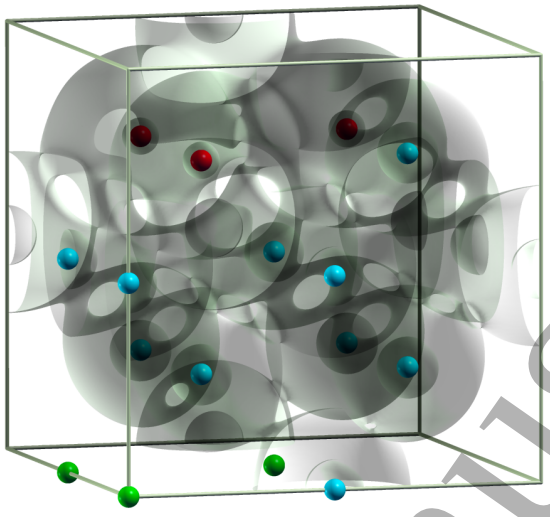

Figure 6: (Colour online) Example electron density isosurface (5×10^{22} cm^{-3}) when excited state PAW potentials are used to model an ensemble of charge states in a plasma. Note that the increasing ion charge states of green $\rightarrow$ blue $\rightarrow$ red (representing 0, 1 and 2 electron holes in the Na L shell) also exhibit increasing electron screening as indicated by the encroaching isosurface.

Angular momentum decomposition for 3 and 4 electron holes in the Na L shell suggests the formation of broad peaks in the DOS, consistent with the formation of atomic-like 3s, 3p and 3d orbitals. The agreement of all-electron calculations with excited core PAW potentials in predicting these structures (previously seen in dense plasma calculations using frozen core, excited [49] and ground state [65] Aluminium PAW potentials) bodes well for the latter as a tool for investigating the role a variety of different charge states may have on the formation of bound states within a plasma.

To highlight the role excited state potentials can play in investigating in detail the local effects of charge state distributions in dense plasmas, we present in Figure 6 a plot of the valence electron density isosurface corresponding to the mean valence charge density, 5×10^{22} cm^{-3}, for a solid-density Na system composed of a range of integer charge states. Taking into account the distribution of charge states present has led to asymmetry in the resulting charge density, even though the ions themselves form a perfect bcc lattice. The tight isosurface spheres surrounding the ions in red, corresponding to ions with 2 holes in the L shell, illustrate how valence electrons are focused tightest around the highest charge states. Meanwhile, the valence density around the ground state Na ions, which have a full L shell and are shown in green, remains relatively low and below the isosurface value of 5×10^{22} cm^{-3}.

We note that appropriate excited potentials have been built by directly enforcing the desired orbital occupancies during the isolated atom stage of PAW potential construction. The isolated atom DFT calculations do not make use of finite temperature DFT. Instead, excited occupations are directly enforced on core states only, allowing

the remaining valence states to achieve their lowest energy occupation (subject to overall charge neutrality). As a result the number of isolated atom K-S orbitals to be computed remains low, and the PAW potential construction process is quick. Ultimately, generating pseudopotentials for generic core occupations will require directly enforcing excited configurations on core atomic K-S orbitals (even if the atomic valence states are to be thermally occupied) and thus our demonstration of the consistency of this method in particular is important for future calculations.

5. Conclusions

An account of thermal fluctuations and local variations in electron charge density remains an important aspect of plasma structure, and is not fully included in finite temperature DFT treatments based on all-electron or ground state pseudopotentials. Excited state potentials offer the possibility to account for such physics by explicitly modelling the ensemble distribution of ion charge states within a plasma. Through comparison with finite temperature, all-electron results we have proposed and demonstrated a consistency test for these pseudopotentials. As an example, excited state PAW potentials passing this test for a range of Na ion charge states have been considered and deployed to model the many charge states present in a plasma via a large supercell DFT calculation. By doing so we have effectively extracted the problem of dealing with excited ion core states and reformatted it as an issue of boundary conditions imposed by pseudopotentials on valence electrons. No doubt an extension of this method across the periodic table would benefit from increased abilities to to perform all-electron calculations at finite temperatures. Our consistency tests here on warm dense Na help legitimise this approach in so far as the core excited states are reachable via finite temperature calculations, and in doing so opens up the door for these excited state potentials to be further studied and ultimately applied to charge state distributions within dense plasmas.

6. Acknowledgements

S.M.V. and J.S.W. are grateful for support from EPSRC under grant number EP/P015794/1. S.M.V is University Research Fellow of the Royal Society.

[1] P. Hohenberg and W. Kohn. Inhomogeneous Electron Gas. *Phys. Rev.*, 136(3B):B864–B871, 1964.

[2] F. Perrot. Model for atomic species in a dense plasma: Description and applications. *Physical Review A*, 35(3), 1987.

[3] M. W. C. Dharma-wardana and Franqois Perrot. Level shifts, continuum lowering, and the mobility edge in dense plasmas. *Physical Review A*, 45(8):5883–5896, 1992.

[4] C E Starrett, J Daligault, and D Saumon. Pseudoatom molecular dynamics. *Physical Review E - Statistical, Nonlinear, and Soft Matter Physics*, 91(1):1–5, 2015.

[5] M. P. Desjarlais, J. D. Kress, and L. A. Collins. Electrical conductivity for warm, dense aluminum plasmas and liquids. *Phys. Rev. E*, 66(2):025401, aug 2002.

[6] Peter E. Blöchl, Johannes Kaestner, and Clemens J. Foerst. Electronic structure methods: Augmented Waves, Pseudopotentials and the Projector Augmented Wave Method. pages 93–94, 2004.

[7] N. David Mermin. Thermal Properties of the Inhomogeneous Electron Gas. *Phys. Rev.*, 137(5A):1–3, 1965.

[8] Travis Sjostrom, Scott Crockett, and Sven Rudin. Multiphase aluminum equations of state via density functional theory. *Physical Review B*, 94(14):1–10, 2016.

[9] N. D. M. Hine, P. D. Haynes, A. A. Mostofi, C.-K. Skylaris, and M. C. Payne. Linear-scaling density-functional theory with tens of thousands of atoms: Expanding the scope and scale of calculations with ONETEP. *Computer Physics Communications*, 180(7):1041–1053, jul 2009.

[10] Ann E Mattsson, Peter A Schultz, Michael P Desjarlais, Thomas R Mattsson, and Kevin Leung. Designing meaningful density functional theory calculations in materials science—a primer. *Modelling and Simulation in Materials Science and Engineering*, 13(1):R1–R31, 2004.

[11] Miguel A. Morales, Lorin X. Benedict, Daniel S. Clark, Eric Schwegler, Isaac Tamblyn, Stanimir A. Bonev, Alfredo A. Correa, and Steven W. Haan. Ab initio calculations of the equation of state of hydrogen in a regime relevant for inertial fusion applications. *High Energy Density Physics*, 8(1):5–12, 2012.

[12] Jean Clérouin, Patrick Renaudin, Yann Laudernet, Pierre Noiret, and Michael P Desjarlais. Electrical conductivity and equation-of-state study of warm dense copper: Measurements and quantum molecular dynamics calculations. *Physical Review B*, 71(6):064203, feb 2005.

[13] N. Nettelmann, B. Holst, A. Kietzmann, M. French, R. Redmer, and D. Blaschke. Ab initio Equation of State data for hydrogen, helium, and water and the internal structure of Jupiter. *The Astrophysical Journal*, 668:1217–1228, dec 2008.

[14] P. M. Kowalski, S. Mazevet, D. Saumon, and M. Challacombe. Equation of state and optical properties of warm dense helium. *Physical Review B - Condensed Matter and Materials Physics*, 76(7):1–14, 2007.

[15] L. Caillabet, S. Mazevet, and P. Loubeyre. Multiphase equation of state of hydrogen from ab initio calculations in the range 0.2 to 5 g/cc up to 10 eV. *Physical Review B - Condensed Matter and Materials Physics*, 83(9), 2011.

[16] Winfried Lorenzen, Bastian Holst, and Ronald Redmer. Demixing of hydrogen and helium at megabar pressures. *Physical Review Letters*, 102(11):1–4, 2009.

[17] Bastian Holst, Ronald Redmer, and Michael P. Desjarlais. Thermophysical properties of warm dense hydrogen using quantum molecular dynamics simulations. *Physical Review B - Condensed Matter and Materials Physics*, 77(18):1–7, 2008.

[18] Michael P. Desjarlais. Quantum Molecular Dynamics Simulations for Generating Equation of State Data. *AIP Conference Proceedings*, 1161(1):32–38, 2009.

[19] Andre Kietzmann, Bastian Holst, Ronald Redmer, Michael P. Desjarlais, and Thomas R. Mattsson. Quantum molecular dynamics simulations for the nonmetal-to-metal transition in fluid helium. *Physical Review Letters*, 98(19):98–101, 2007.

[20] Travis Sjostrom and Scott Crockett. Quantum molecular dynamics of warm dense iron and a five-phase equation of state. *Physical Review E*, 97(5), may 2018.

[21] T. G. White, S. Richardson, B. J B Crowley, L. K. Pattison, J. W O Harris, and G. Gregori. Orbital-free density-functional theory simulations of the dynamic structure factor of warm dense aluminum. *Physical Review Letters*, 111(17):1–5, 2013.

[22] Hannes R. Rüter and Ronald Redmer. Ab initio simulations for the ion-ion structure factor of warm dense aluminum. *Physical Review Letters*, 112(14):145007, apr 2014.

[23] T. R. Mattsson and M. P. Desjarlais. Phase Diagram and Electrical Conductivity of High Energy-Density Water from Density Functional Theory. *Physical Review Letters*, 97(1):017801, jul 2006.

[24] Flavien Lambert, Vanina Recoules, Alain Decoster, Jean Clerouin, and Michael Desjarlais. On the transport coefficients of hydrogen in the inertial confinement fusion regime. *Physics of Plasmas*, 18(5):056306, 2011.

[25] B. B.L. Witte, L. B. Fletcher, E. Galtier, E. Gamboa, H. J. Lee, U. Zastrau, R. Redmer, S. H. Glenzer, and P. Sperling. Warm Dense Matter Demonstrating Non-Drude Conductivity from Observations of Nonlinear Plasmon Damping. *Physical Review Letters*, 118(22):225001, 2017.

[26] M. W.C. Dharma-Wardana, D. D. Klug, L. Harbour, and Laurent J. Lewis. Isochoric, isobaric, and ultrafast conductivities of aluminum, lithium, and carbon in the warm dense matter regime. *Physical Review E*, 96(5):1–15, 2017.

[27] S Mazevet, L. A. Collins, N. H. Magee, J. D. Kress, and J. J. Keady. Quantum molecular dynamics calculations of radiative opacities. *Astronomy and Astrophysics*, 405(1):5–9, 2003.

[28] P Hollebon, O Ciricosta, M P Desjarlais, C Cacho, C Spindloe, E Springate, I. C.E. Turcu, J S Wark, and S M Vinko. Ab initio simulations and measurements of the free-free opacity in aluminum. *Physical Review E*, 100(4):43207, 2019.

[29] S. Mazevet, M. P. Desjarlais, L. A. Collins, J. D. Kress, and N. H. Magee. Simulations of the optical properties of warm dense aluminum. *Phys. Rev. E*, 71(1):016409, jan 2005.

[30] S. Mazevet, J. Clérouin, V. Recoules, P. M. Anglade, and G. Zerah. Ab-Initio Simulations of the Optical Properties of Warm Dense Gold. *Phys. Rev. Lett.*, 95(8):085002, aug 2005.

[31] Michael P. Desjarlais. First-principles calculation of entropy for liquid metals. *Physical Review E*, 88(6):062145, dec 2013.

[32] Martin French, Andreas Becker, Winfried Lorenzen, Nadine Nettelmann, Mandy Bethkenhagen, Johannes Wicht, and Ronald Redmer. Ab Initio Simulations for Material Properties Along the Jupiter Adiabat. *The Astrophysical Journal Supplement Series*, 202(1):5, 2012.

[33] W. Kohn and L. J. Sham. Self-Consistent Equations Including Exchange and Correlation Effects. *Phys. Rev.*, 140(4A):1133, 1965.

[34] Carlos A. Iglesias and Philip A. Sterne. Fluctuations and the ionization potential in dense plasmas. *High Energy Density Physics*, 9(1):103–107, 2013.

[35] Chengliang Lin, Gerd Röpke, Wolf Dietrich Kraeft, and Heidi Reinholz. Ionization-potential depression and dynamical structure factor in dense plasmas. *Phys. Rev. E*, 96(1):013202, 2017.

[36] B. Kramer and A. MacKinnon. Localization: theory and experiment. *Reports on Progress in Physics*, 56(12):1469, 1993.

[37] Pier Luigi Silvestrelli. No evidence of a metal-insulator transition in dense hot aluminum: A first-principles study. *Phys. Rev. B*, 60(24):16382–16388, 1999.

[38] Ronald Redmer, Gerd Röpke, Sandra Kuhlbrodt, and Heidi Reinholz. Hopping conductivity in dense hydrogen fluid. *Physical Review B - Condensed Matter and Materials Physics*, 63(23), 2001.

[39] G. Röpke, H. Reinholz, C. Neißner, B. Omar, and a. Sengebusch. Bound State Formation and Optical Properties of Partially Ionized Dense Plasmas. *Contributions to Plasma Physics*, 45(5-6):414–423, 2005.

[40] B. J. B. Crowley. Continuum lowering - A new perspective. *High Energy Density Physics*, 13(1):84–102, 2014.

[41] M. W.C. Dharma-wardana. Current issues in finite-T density-functional theory and warm-correlated matter. *Computation*, 4(2):16, 2016.

[42] E Pehlke and M Scheffler. Evidence for site-sensitive screening of core holes at the Si and Ge (001) surface. *Physical Review Letters*, 71(14):2338–2341, 1993.

[43] Jun-Hyung Cho, Sukmin Jeong, and Myung-Ho Kang. Final-state pseudopotential theory for the Ge 3d core-level shifts on the Ge/Si (100)-(2× 1) surface. *Physical Review B*, 50(23):0–3, 1994.

[44] Alfredo Pasquarello, M. S. Hybertsen, and Roberto Car. Theory of Si 2p core-level shifts at the Si(001)-SiO2 interface. *Physical Review B*, 53(16):10942–10950, apr 1996.

[45] S. Mazevet and G. Zérah. Ab Initio Simulations of the K-Edge Shift along the Aluminum Hugoniot. *Physical Review Letters*, 101(15):155001, oct 2008.

[46] A. Benuzzi-Mounaix, F. Dorchies, V. Recoules, F. Festa, O. Peyrusse, A. Levy, A. Ravasio, T. Hall, M. Koenig, N. Amadou, E. Brambrink, and S. Mazevet. Electronic structure investigation of highly compressed aluminum with K edge absorption spectroscopy. *Physical Review Letters*, 107(16):165006, oct 2011.

[47] V. Recoules and S. Mazevet. Temperature and density dependence of XANES spectra in warm dense aluminum plasmas. *Physical Review B*, 80(6):064110, aug 2009.

[48] S. M. Vinko, U. Zastrau, S. Mazevet, J. Andreasson, S. Bajt, T. Burian, J. Chalupsky, H. N. Chapman, J. Cihelka, D. Doria, T. Döppner, S. Düsterer, T. Dzelzainis, R. R. Fäustlin, C. Fortmann, E. Förster, E. Galtier, S. H. Glenzer, S. Göde, G. Gregori, J. Hajdu, V. Hajkova, P. A. Heimann, R. Irsig, L. Juha, M. Jurek, J. Krzywinski, T. Laarmann, H. J. Lee, R. W. Lee, B. Li, K. H. Meiwes-Broer, J. P. Mithen, B. Nagler, A. J. Nelson, A. Przystawik, R. Redmer, D. Riley, F. Rosmej, R. Sobierajski, F. Tavella, R. Thiele, J. Tiggesbäumker, S. Toleikis, T. Tschentscher, L. Vysin, T. J. Whitcher, S. White, and J. S. Wark. Electronic Structure of an XUV Photogenerated Solid-Density Aluminum Plasma. *Physical Review Letters*, 104(22):2–5, 2010.

[49] S. M. Vinko, O Ciricosta, and J. S. Wark. Density functional theory calculations of continuum lowering in strongly coupled plasmas. *Nature communications*, 5:3533, jan 2014.

[50] O. Ciricosta et al. Direct Measurements of the Ionization Potential Depression in a Dense Plasma. *Physical Review Letters*, 109(6):065002, 2012.

[51] O. Ciricosta et al. Detailed model for hot-dense aluminum plasmas generated by an x-ray free electron laser. *Phys. Plasmas*, 23(2), 2016.

[52] O. Ciricosta et al. Measurements of continuum lowering in solid-density plasmas created from elements and compounds. *Nat. Commun.*, 7:11713, 05 2016.

[53] S. H. Glenzer and R. Redmer. X-ray Thomson scattering in high energy density plasmas. *Rev. Mod. Phys.*, 81:1625–1663, 2009.

[54] S. Toleikis et al. Probing near-solid density plasmas using soft x-ray scattering. *Journal of Physics B: Atomic, Molecular and Optical Physics*, 43(19):194017, 2010.

[55] O. S. Humphries, R. S. Marjoribanks, Q. Y. van den Berg, E. C. Galtier, M. F. Kasim, H. J. Lee, A. J. F. Miscampbell, B. Nagler, R. Royle, J. S. Wark, and S. M. Vinko. Probing the electronic structure of warm dense nickel via resonant inelastic x-ray scattering. *Phys. Rev. Lett.*, 125:195001, 2020.

[56] X. Gonze, B. Amadon, P.-M. Anglade, J.-M. Beuken, F. Bottin, P. Boulanger, F. Bruneval, D. Caliste, R. Caracas, M. Côté, T. Deutsch, L. Genovese, Ph. Ghosez, M. Giantomassi, S. Goedecker, D. R. Hamann, P. Hermet, F. Jollet, G. Jomard, S. Leroux, M. Mancini, S. Mazevet, M. J. T. Oliveira, G. Onida, Y. Pouillon, T. Rangel, G.-M. Rignanese, D. Sangalli, R. Shaltaf, M. Torrent, M. J. Verstraete, G. Zerah, and J. W. Zwanziger. ABINIT: First-principles approach to material and nanosystem properties. *Computer Physics Communications*, 180(12):2582–2615, dec 2009.

[57] P. E. Blöchl. Projector augmented-wave method. *Phys. Rev. B*, 50(24):17953–17979, 1994.

[58] N. A. W. Holzwarth, A. R. Tackett, and G. E. Matthews. A Projector Augmented Wave (PAW) code for electronic structure calculations, Part I: atompaw for generating atom-centered functions. *Computer Physics Communications*, 135(3):329–347, apr 2001.

[59] Riccardo Gusmeroli and Claudia Dallera. Missing, http://www.esrf.eu/computing/scientific/MISSING/.

[60] R. D. Cowan. *The Theory of Atomic Structure and Spectra*. University of California Press, 1981.

[61] John P. Perdew, Kieron Burke, and Matthias Ernzerhof. Generalized Gradient Approximation Made Simple. *Physical Review Letters*, 77(18):3865–3868, oct 1996.

[62] Hendrik J Monkhorst and James D Pack. Special points for Brillonin-zone integrations. *Physical Review B*, 13(12):5188–5192, 1976.

[63] C. S. Barrett. X-ray study of the alkali metals at low temperatures. *Acta Crystallographica*, 9(8):671–677, 1956.

[64] U. von Barth and C. D. Gelatt. Validity of the frozen-core approximation and pseudopotential theory for cohesive energy caluclations. *Physical Review B*, 21(6):2222, 1980.

[65] A. Lévy, F. Dorchies, A. Benuzzi-Mounaix, A. Ravasio, F. Festa, V. Recoules, O. Peyrusse, N. Amadou, E. Brambrink, T. Hall, M. Koenig, and S. Mazevet. X-Ray Diagnosis of the Pressure Induced Mott Nonmetal-Metal Transition. *Physical Review Letters*, 108(5):055002, 2012.